Vertical temperature profiles in the Venus mesosphere obtained by two retrieval methods from the VIRTIS-VEX observations

Paulina Wolkenberg , Giuseppe Piccioni , Marek Banaszkiewicz

PII: S0022-4073(17)30160-7
DOI: 10.1016/j.jqsrt.2018.06.010
Reference: JQSRT 6133

To appear in: *Journal of Quantitative Spectroscopy & Radiative Transfer*

Received date: 21 February 2017
Revised date: 12 June 2018
Accepted date: 12 June 2018

Please cite this article as: Paulina Wolkenberg , Giuseppe Piccioni , Marek Banaszkiewicz , Vertical temperature profiles in the Venus mesosphere obtained by two retrieval methods from the VIRTIS-VEX observations, *Journal of Quantitative Spectroscopy & Radiative Transfer* (2018), doi: 10.1016/j.jqsrt.2018.06.010

Highlights

- VIRTIS(M)-VEX measurements are used to retrieve mesospheric temperature profiles.
- Results for two independent retrieval methods (Chahine, Bayes) are compared.
- Temperature profiles are in good agreement for both algorithms.
- Corresponding standard deviations do not exceed 5 K for altitudes above 59 km.
- Cold collar and hot polar regions are observed.

Vertical temperature profiles in the Venus mesosphere obtained by two retrieval methods from the VIRTIS-VEX observations

by

Paulina Wolkenberg[1,2], Giuseppe Piccioni[1]

and Marek Banaszkiewicz[2]

Corresponding Author:

Paulina Wolkenberg: paulina@cbk.waw.pl, paulina.wolkenberg@iaps.inaf.it

[1]Istituto di Astrofisica e Planetologia Spaziali (IAPS) – Istituto Nazionale di Astrofisica (INAF), Via del Fosso del Cavaliere 100, Roma, Italy

[2]Space Research Centre of the Polish Academy of Sciences, ul. Bartycka 18A, 00-716 Warsaw, Poland

Abstract

We present vertical temperature profiles derived by two different retrieval methods from nighttime radiation measurements performed by VIRTIS(M)-VEx (Visible and Infrared Thermal Imaging Spectrometer, M channel – Venus Express). The Bayesian approach to the optimal estimation method and the relaxation method are applied in this study. This is a first attempt to present and compare results obtained from two independent methods. It allows us to be more convinced of our interpretation.

After comparison of temperature profiles we conclude that both retrieval methods are able to sound the atmospheric layers higher than 59 km (<150 mb) with a single-standard deviation error of less than 5 K at the bottom and even deeper for some measurements down to 56 km but with error larger than 10 K. The best consistency between temperature profiles obtained from the two algorithms with the standard deviation less than 2.5 K is observed for atmospheric layers between 70 km – 77 km (15 – 3.5 mb).

In our conclusion we have no preference for any approach. Two methodologies are of equivalent value. Both methods resolve temperature inversions at high altitudes (~84 km), the quality of fits for all observations is equally well. Only for the Bayesian approach, the retrieval uncertainty above 62 km up to 95 km is less than 2 K. A disadvantage of this method is the time-consuming calculation of weighting functions.

The atmospheric temperatures over the "cold collar" region located at 60°S – 75°S (60 - 70 km) are ~10 K smaller than for latitudes poleward of 75°S (polar region). The cold collar region is seen very clearly in our results for both methods.

1. Introduction

Temperature is one of main atmospheric variables used in meteorology and chemistry of planetary atmospheres to constrain present models. The Venus atmosphere with respect to a vertical variation of temperature can be divided into three main layers including the troposphere (0 – 60 km), the mesosphere (60 – 100 km), and the thermosphere (above 100 km) (Svedhem et al., 2009). Venus has no stratosphere, there is a tropopause which appears at altitudes from ~55 km to 62 km dependent on latitude, defined as a point of sudden change in the temperature lapse rate. The thermal structure of Venus had been observed by many instruments in-situ or remotely by infrared spectroscopy, radio and stellar occultation measurements (Haus et al., 2013).

The Pioneer Venus observations (Taylor et al., 1980) provided the first view of the mesospheric structure and dynamics extending from 60 km (~150 mb) to 100 km (~0.02 mb) (Bougher et al., 1997). The most characteristic features of Venus' mesosphere are the "cold collar" zones at 60° to 75° latitude below 70 km (Taylor et al., 1980) and hot polar regions. Temperatures observed by Pioneer Venus (PV) decreased slightly from the equator to the "cold collar" region below 70 km. In the northern "cold collar" PV temperatures were ~30 K smaller than at the equator at ~67 km. The VIRTIS instrument (Visible and Infrared Thermal Imaging Spectrometer) also investigated the southern polar features (Piccioni et al., 2007a) and found high similarities to those observed in the north by previous missions. In the "cold collar" region centered at 65°S at 62 km (100 mb) (Grassi et al., 2008; 2010), the 20 K temperature inversion was detected below 70 km (~15 mb). Similar cold collar characteristics were also observed by the Venus Express Radio Science experiment (VeRa) sounded the Venusian atmosphere from 40 – 90 km (Tellmann et al. 2009, 2012) and Galileo NIMS (Near Infrared Mapping Spectrometer) (Roos – Serote et al., 1995).

Retrieved temperature profiles obtained from PV, NIMS, VeRa, and VIRTIS experiments have shown an inverted equator-to-pole gradient between 70 and 100 km and poleward of the "cold collar", that is, the poles are warmer than the equator by about 10-15 K at altitudes above 70 km. This anomaly is associated with the disappearance of the cloud-top

superrotation (Bougher et al., 1997). Poleward of 75°S and at altitudes between 60 and 70 km, VIRTIS temperatures varied weakly with height, they were quasi-isothermal (Piccioni et al., 2007a, Grassi et al., 2008; 2010, Haus et al., 2014).

Usually the information on atmospheric temperatures is drawn from indirect measurements. Temperature is not straightforward measured by sensors but is retrieved from the radiance spectra using one of the existing inversion methods. For the Venus atmosphere vertical temperature profiles can be inferred from radiances measured in two CO_2 absorption bands at 4.3 μm and 15 μm. The inversion of radiative transfer equation is an 'ill-posed' problem and the direct inversion is usually unstable and nonlinear. Thus, it is necessary the 'ill-posed' problem converges to 'well posed', it is necessary to take into account additional constraints on possible solutions derived from certain a priori information. The 'ill-posed' problem can then be solved by applying different retrieval techniques that fall into two main classes: 'statistical' and 'relaxation' methods. Relaxation techniques were described by Smith (1970), Chahine (1970). The Bayesian approach with optimal estimation method (Rodgers, 2000) is among most frequently used statistical techniques.

In this study we use two retrieval methods to obtain vertical temperature profiles from the nighttime VIRTIS(M) – VEX observations. We present a preliminary comparison of temperature profiles retrieved by the Bayesian approach (Rodgers, 2000) which was also implemented by Grassi et al. (2014) and the Chahine's method adopted to the Venus atmosphere (Chahine, 1970; Zasova et al., 1999; Grassi et al., 2008). We retrieve temperature profiles from 56 km (~300 mb) to 98 km (~0.03 mb). The goal of this study is to investigate the results of retrieval process for these two methods. It is of special importance to compare retrieved temperature profiles at altitudes between 50 and 70 km where the clouds significantly contribute to the total atmospheric opacity.

2. Observations – VIRTIS-M data

The VIRTIS-M spectro-imager measured radiation emerging from the atmosphere and provided spectra from the spectral range from 1000 nm to 5100 nm with the sampling step 9.5 nm. Instantaneous field of view for the VIRTIS-M was 0.25 mrad x 0.25 mrad (Piccioni et al., 2007b; Grassi et al., 2008; Grassi et al., 2014).

We constrain our study to the nighttime data because our model cannot deal with scattered sunlight and CO_2 non-LTE emission occurring at VIRTIS wavelengths on the dayside. Measurements were downloaded from the ESA website (ftp://psa.esac.esa.int/pub/mirror/VENUS-EXPRESS/VIRTIS/VEX-V-VIRTIS-2-3-v3.0). We selected measurements from the southern hemisphere, always one observation within a latitude belt of 5° starting from the equator down to the South Pole. This way, we obtain 18 measurements for the entire hemisphere. Table 1 presents some parameters of these observations.

3. Atmospheric model and forward radiative transfer model

Monochromatic radiances at the top of atmosphere are computed by means of the DISORT package (Stamnes et al., 1988). The DISORT code takes into account the multiple scattering of radiation through a plane-parallel stratified atmosphere. In order to calculate the model spectral radiances, we use the adopted version of DISORT described by García-Muñoz et al. (2013). DISORT considers only one wavelength, thus the adopted code includes the spectral range used for the retrieval of temperature profiles. Moreover, a look up table with aerosol for Venus and a range of temperatures and pressures were taken into account. Our forward radiative transfer model computes radiances considering 50 layers from 50 km to 100 km with 1 km sampling. The model atmosphere is mainly composed of CO_2 (96.5%) and N_2 (3.5%). The gas and aerosol optical properties were calculated separately and then tabulated in order to use them as look-up tables during the retrieval procedure. The CO_2 line parameters like intensity, position and width at T = 296 K are taken from the HITRAN 2008 database (Rothman et al., 2009). The Voigt line-shape with a 200 cm^{-1} cut off is assumed considering a sub-Lorentzian modification of line wings beyond 5 cm^{-1} according to Winters (1964). The gas absorption coefficients are calculated for the pressure range from 10 to 10^{-8} bar and the temperature range from 140 to 400 K with 10 K step leading to 27 temperature levels linearly spaced. They are stored as a table. Each ten-fold change in pressure is divided to 4 levels, so the total number of layers is 36. The pre-calculated gas optical properties are linearly interpolated to the 51 altitude steps used in the radiative transfer calculations. The optical properties for aerosol are computed on the basis of Mie theory.

Aerosols (clouds) on Venus are vertically stratified and composed of three main layers possessing at least three different particle sizes referred to as modes (Carlson et al., 1993).

Mode 1 contains particles with average diameters of 0.6 μm observed mainly in the upper cloud layer with less concentration in the middle and lower cloud regions. Mode 2 and 2' have particles with diameters approximately of 2 and 3 μm, respectively. Mode 2 is observed rather in the upper cloud layer. Mode 2' with larger particles occur in the lower and middle cloud regions. The largest particle sizes with diameters around 7 μm (mode 3) are found in lower and middle cloud layers (Carlson et al., 1993).

In this work, log-normal aerosol particle size distributions are used considering only mode 2 particles with r_{eff} = 1.09 μm (r_{mod} = 1.0 μm) and variances v_{eff} = 0.037 (σ = 1.21) (Molaverdikhani et al., 2012). The choice of only mode 2 aerosols is suggested by studies on an effect of different modes on model spectra performed by Haus et al. (2013) and García-Muñoz et al. (2013). Wings of CO_2 absorption band at 4.3 μm are mainly sensitive to mode 2 cloud particles while other modes have only small influences on radiances and resulting brightness temperatures in the considered spectral range. Different size distributions than mode 2 have negligible effect on brightness temperatures in the considered spectral range.

The cloud chemical composition with the 84.5% of H_2SO_4 by weight in the solution with H_2O (Molaverdikhani et al., 2012) is assumed with refractive indices given by Palmer and Williams (1975). The model vertical distribution of aerosol is assumed as an exponential decrease in number density dependent on z_{ct} and H described by García-Muñoz et al. (2013):

$$N(z') = \frac{exp\left(-\frac{z'-z_{ct}}{H}\right)}{\sigma_{\tilde{\lambda}} H} \quad (1)$$

where z' is the transformed atmospheric altitude at the 51 model layer boundaries between 50 and 100 km, starting at z'=z-50 km. z_{ct} is the cloud top altitude, H is the cloud scale height and $\sigma_{\tilde{\lambda}} = 6 \cdot 10^{-8}$ cm^2 is the aerosol extinction cross-section at $\tilde{\lambda}$ = 4.81 μm taken from Lee (2012a). This means that the optical depth at z'=z_{ct} (total optical depth above level z') at this wavelength is equal to 1.0, and the atmosphere becomes opaque at levels $z' < z_{ct}$. The altitude z is the altitude at 50 layer boundaries. During a retrieval calculation, the cloud properties are assumed as a constant value but they change with latitude as given in Tab.2. We assume the cloud parameters (H and z_{ct}) to be based on results obtained by Lee (2012a); Lee et al. (2012b) because they were derived from VIRTIS observations at 4.65 and 5 μm. The altimetry of clouds is also presented by Ignatiev et al. (2009) but it is inferred from VIRTIS dayside measurements in the 1.6 μm spectral range. They show higher values of z_{ct} around 5

km than those calculated at 8.21 µm (Zasova et al., 1999) from the Venera 15 mission. Because of the spectral variation of H and z_{ct} we decide to use estimated values for cloud properties derived by Lee et al. 2012b from the spectral range which we use for the retrieval of temperature profiles.

Synthetic spectra are calculated for the spectral range from 3917 nm to 5555 nm (1800 - 2553 cm^{-1}).

The wavenumber grid is not linearly spaced in the line by line calculation. It is built according to a geometrical summation rule assuming that the ratio $\frac{\Delta\nu}{\nu}$ of bin size and mid-wavenumber within the bin is constant.

It was shown by García-Muñoz et al. (2013) that a moderate spectral grid consisting of 22000 points is sufficient to produce reliable results, and that this grid induces negligible errors in the order of 1% in the synthetic spectra compared to a much finer wavenumber grid (1.1 x 10^6 points). The atmospheric trace gas CO with absorption features in the 2100-2200 cm^{-1} range is not taken into account in the retrieval process. Other trace gases like H_2O, SO_2, and OCS can be safely neglected near 4.3 µm due to very low absorption cross-sections compared to CO_2.

Temperature retrieval procedures require the definition of initial temperature profiles. Fig. 1 shows a selection of latitude-dependent profiles which are taken from VIRA2 (Zasova et al., 2006). The profile denoted as 'true' is the profile that is used in both applied retrieval methods to determine their retrieval uncertainty (see Sections 4 and 5). It is similar to the selected polar profiles, but has a slightly stronger inversion near 60 km. The meaning of the 'a priori' profile is explained later on in Section 5.

4. Chahine method adopted to the Venus atmosphere

Derivation of *T(p)* is associated with the fact the radiative transfer equation in the integral form may not always have a solution for an arbitrary radiance function (Chahine, 1970). The reduction of this problem to linear system of equations is inappropriate from the mathematical point of view. Thus, one of nonlinear approaches described by Chahine (1970) is necessary.

This method allows to reconstruct *T(p)* from a relation between simulated and measured radiances for defined wavelengths and altitudes. Assuming a weak dependence of atmospheric transmission functions on changes in temperature, Chahine derived an equation of the form:

$$\frac{I^n(\lambda_j,p)}{\tilde{I}(\lambda_j)} \cong \frac{I_B\left(\lambda_j,x^n(p_j)\right)}{I_B\left(\lambda_j,x^{n+1}(p_j)\right)} \qquad (2)$$

where:

λ_j is the wavelength at which radiance reaches maximum at pressure level p_j;

$I^n(\lambda_j,p)$ is the calculated radiance at wavelength λ_j and at p-th pressure level for n-th iteration;

$\tilde{I}(\lambda_j)$ is the measured radiance at wavelength λ_j;

$x^n(p_j)$ is the temperature at p_j for n-th iteration;

$x^{n+1}(p_j)$ is the temperature at p_j for $n+1$-th iteration;

$I_B\left(\lambda_j,x^n(p_j)\right)$ is the Planck blackbody function for $x^n(p_j)$;

$I_B\left(\lambda_j,x^{n+1}(p_j)\right)$ is the Planck blackbody function for $x^{n+1}(p_j)$.

$x(p_j)$ is represented by a linear interpolation between p_j levels. From Eq.2 we can derive the $x^{n+1}(p_j)$ for $n+1$-th iteration. This version of the approach was applied by Roos-Serote et al. (1995) for Galileo NIMS spectra.

In this study we utilize the modified version of Chahine method as described by Zasova et al. (1999). This method was also used by Grassi et al. (2008). The difference between the original version of the method and that presented here is that spectral radiances are changed to brightness temperatures, and the temperature at each pressure level is weighted by weighting functions $W_n(p)$ defined as the derivative of wavelength-dependent atmospheric column transmittances above a pressure reference level with respect to the logarithm of pressure. This leads to an equation of the form:

$$x^{n+1}(p) = x^n(p)\frac{\sum_{j=1}^{k}\left(\frac{B_j^*}{B_j}W_j^n(p)\right)}{\sum_{j=1}^{k}W_j^n(p)} \qquad (3)$$

where $x^{n+1}(p)$ is the temperature at pressure level p at $n+1$-th iteration, B_j^* and B_j are the observed brightness temperatures at wavelength channel j, respectively and k is the total number of channels. Weighting functions $W^{(n)}{}_j(p)$ are recalculated at each iteration step for each new temperature profile.

Introduction of these weighting functions accounts for the fact that atmospheric transmittances usually strongly depend on changes of temperature profiles. The weighting functions determine the effective pressure (altitude) range of temperature sounding, since

maximum temperature information at a certain wavelength comes from the altitude where the maximum of $W^{(n)}{}_j(p)$ is located. Examples of weighing functions at selected wavelengths are shown in Fig. 2a (see Section 5 with respect to Fig. 2b).

However, there are limitations of two methods due to missing weighting function information, particularly below 60 km. In the Chahine method, the maximum of weighting function at 5.08 μm is at 61 km. However, weighting functions contribute to the emerging radiance from atmospheric layers above 53 km (Fig. 2a). It is also interesting to note that some contributions to the weighting functions originate in upper atmospheric layers above 90 km. These contributions could allow us to sound atmospheric temperatures up to 98 km but the large noise in the bottom of CO_2 absorption band and less dense atmosphere prevents to retrieve reliable temperatures. We have checked the effect of temperature profiles at boundaries by assuming that the contribution of weighting functions at certain atmospheric levels is equalled to 0. This forces that retrieved temperature profiles at boundaries converge to the initial temperature profiles. After tests for the convergence to initial profiles at the bottom and for upper atmospheric layers we find that above around 90 km (0.2 mb) temperature profiles do not affect significantly (within noise) simulated brightness temperatures in the centre of CO_2 band for considered measurements. At the bottom we observe that temperature profiles converge to initial profiles at around 56 km (300 mb) for equatorial and mid-latitude measurements, and at around 60 km for "cold collar" and polar regions without significant changes of brightness temperatures in the modelled spectra.

In this study, we apply the approach to estimate the temperature uncertainty using given NER (noise equivalent radiance). For this purpose, we first calculate the radiance (R) for a known temperature profile $T(p)$. The profile 'true' from Fig. 1 is used here. In the next step we generate random Gaussian noise with a wavelength-independent standard deviation of $5 \cdot 10^{-4}$ W / (m^2 sr μm), which corresponds to the approximate noise equivalent radiance of 4.3 μm VIRTIS measurements (Grassi et al., 2008). This way, we fix 10 spectra to be generated applying different (synthetic) NER for different standard deviations. In the next step we calculate brightness temperatures for the radiances (R) applying Planck's equation (Fig. 3) and then retrieve temperature profiles according to Eq.(3). Then we seek the best fit between spectral radiances computed for temperature profile $T(p)$ and the radiances determined from the retrieval procedure. The quality of brightness temperature fits is derived

from the root mean square deviation (rmsd) between observed B_j* and modeled B_j brightness temperatures according to the expression:

$$\chi = \sqrt{\frac{\sum_j^k \left(B_j^* - B_j\right)^2}{k}} \qquad (4)$$

where k is the number of spectral channels. We calculate χ for the spectral range from 4.2 – 5.1 μm. We exclude the CO range from 2100-2200 cm^{-1} (4.55 - 4.76 μm) in the fitting procedure. The differences of 'true' and retrieved temperature profiles are denoted as retrieval uncertainty or retrieval error. This altitude-dependent error is visualized in Fig. 4 for both retrieval methods (with respect to Bayesian approach see Section 5).

During this error estimation, the cloud parameters scale height H and cloud top altitude z_{ct} are held constant, specifically we assume that H = 3.8 km and z_{ct} = 70 km. This assumption is consistent with the cloud model applied in the estimation of temperature uncertainty for the Bayesian approach (section 5).

Fig.4 shows that the retrieval error is less than 2 K for altitude ranges above 58 km (~200 mb) to 74 km (~5 mb) and from 81 km (~1 mb) to 95 km (~0.04 mb). This is a good result. The increase of temperature uncertainty from 2 K to 4 K is observed between 74 km and 81 km with maximum at 78 km (Fig.4). Below 58 km the retrieval uncertainty increases up to 6 K at 56 km. Above 95 km the retrieval error increases to 4 K.

Initial temperature profiles are presented in Fig.1 to retrieve latitude-dependent profiles from latitude-dependent VIRTIS measurements using both methods.

5. Bayesian approach

The radiative transfer equation can be described by a relation between the measurement vector (y) and the state vector (x) according to the formula (Rodgers, 2000):

$$y = F(x) + \varepsilon \qquad (5)$$

The measurement y maps the state (x) into the measurement space through the forward model $F(x)$ but in the presence of the measurement noise ε, which is characterized by a probability density function (*pdf*). In the same way, the prior information about the state can be described by a *pdf*. $P(x)$ is the a priori *pdf* of the state representing the knowledge about state before the measurement, $P(y)$ is the a priori *pdf* of the measurement, $P(x,y)$ is the joint a priori *pdf* of x and y meaning that $P(x,y)dxdy$ is the probability that x lies in $(x,x+dx)$ and y lies in $(y,y+dy)$,

P(y|x) is the *pdf* of the measurement given the state (it describes the forward function with experimental error), and *P(x|y)* is the *pdf* of the state given the measurement, that is, the wanted function.

Then Bayes' theorem states that $P(x|y) = P(y|x)P(x)/P(y)$. We want to determine the location of the maximum of the 'a posteriori' *pdf* (that is $P(x|y)$), because this is the most probable state that is compatible with both the measurement error distribution and the a priori parameter distribution. This value for x is searched for instance with the Levenberg-Marquardt algorithm.

We assume that $P(x)$ and $P(y|x)$ are Gaussians. In order to find the state vector x we need to determine the location of the global maximum of the a posteriori *pdf* $P(x|y)$, i.e. the location of the global minimum of the cost function J (eq. 6):

$$J = \left[y - F(x)\right]^T S_e^{-1}\left[y - F(x)\right] + \left[x - x_a\right]^T S_a^{-1}\left[x - x_a\right] \quad (6)$$

where: y – measurement, $F(x)$ – forward model, S_e – covariance matrix of measurement noise (assumed to be diagonal), S_a – *a priori* covariance matrix, x_a – a priori state vector x.

We may have many local minima but we look for the global one by checking the stability of any results against modifications of the initial guess and the a priori data. To find the global minimum, not a subsidiary minimum we apply the Levenberg-Marquardt method. The formula used for finding of the updated vector state x_{n+1} was given from Rodgers (2000) eq. (5.36):

$$x_{n+1} = x_n + \left[(1+\gamma)S_a^{-1} + K_n^T S_e^{-1} K_n\right]^{-1}\left\{K_n^T S_e^{-1}\left[y - F(x_n)\right] - S_a^{-1}\left[x_n - x_a\right]\right\} \quad (7)$$

where:

x_n – the state vector at iteration n comprising the temperatures of the 50 altitude layers

γ – the Levenberg-Marquardt parameter,

K_n – weighting function matrix at n*th* iteration

K_n^T- transposed weighting function matrix at n*th* - iteration,

$F(x_n)$ – forward model.

This is an iterative method and we start with an initial guess for x, that is x_0. Parameter gamma is a line search parameter that is increased when χ^2 increases from one iteration to the next one and decreased when χ^2 decreases with iterations to find the balance between high stability but slow convergence (i.e. steepest descent method) and fast convergence but possible instability (i.e. Gauss-Newton). The χ^2 is defined as:

$$\chi^2 = \frac{1}{N-M}\sum_i^N \left(\frac{F_i - y_i}{NER_i}\right)^2 \quad (8)$$

where: N – total number of spectral measurements, M – degree of freedom, F_i – model radiance at i-th wavelength, y_i – measured radiance at i-th wavelength.

However, after some trials we modify this method and we fix γ as a constant parameter equaled 50 during the retrieval process.

Eq. 7 allows us to compute the state vector x_n during the iterative procedure from step n to step n+1. The final state vector x_n describes our best estimation of the temperature profile based on the 'a priori' information, the measurements y and covariance matrix of measurement noise (S_e). The forward model calculates synthetic spectra for the state vector x_n using the radiative transfer code described in section 3. K_n are the weighting functions described in details further, namely the Jacobian of the forward model with regards to temperature profile (x_n), which is calculated at each iteration step (n).

The S_a, S_e and x_a are defined by physical conditions. 'A priori' data (S_a and x_a) are given here by Venus climatology, that is, a statistical description of already known atmospheric features. S_a is associated with deviation of temperature profile from 'a priori' x_a, and S_e models the difference between measurement y and $F(x_n)$ and is given by parameters of the VIRTIS instrument (especially measurement noise). The covariance matrix S_a for 'a priori' temperature profile (x_a) is determined according to the formula given in Grassi et al. (2014):

$$S_a = \sigma_n \cdot \sigma_m \cdot exp\left[\frac{-(z_n - z_m)^2}{h_c^2}\right] \quad (9)$$

where: $\sigma_n = \sigma_m = 4$ K, z_n, z_m – altitudes at n and m pressure levels, $h_c = 7.5$ km. The covariance matrix can be also calculated from the database of some temperature profiles taken from the Pioneer Venus measurements, VIRA (Kliore et., 1985, Seiff et al., 1983) and VIRA2 (Zasova et al., 2006; 2007). In this study, the 'a priori' temperature profile (x_a) is calculated as a mean temperature profile of selected profiles from the three above mentioned databases. It is shown in Fig.1. This allows us to have a representative 'a priori' temperature profile for all possible atmospheric conditions on Venus. The 'a priori' temperature profile is different from the initial temperature profile and is constant during the retrieval process. The initial temperature profile is chosen from VIRA2 as a nearest one to the measurement location (Fig.1).

In the eq. (7) there is a quantity K_n which is the weighting function matrix. Each element of the *K* matrix is the partial derivative of a forward model element *F(x)* with respect to a state vector element *x*, $K_{jm} = \delta F_j(x)/\delta x_m$ where *j* is the number of the spectral channel and *m* is the number of the atmospheric layer. In order to numerically calculate the derivative we use the perturbation method for the temperature profile. We perturb the temperature of each atmospheric layer considered in this study. For instance, for each of the 51 layer boundaries we change the temperature profile by 1%. The calculation of the weighting function matrix is time-consuming because it requires the evaluation of radiances for temperature profiles with a temperature perturbation for each atmospheric layer. Thus, in one iteration we need to calculate radiances for 52 different temperature profiles including the unperturbed radiance spectrum as well. One example of weighting function matrices is given in Fig. 2b.

The covariance matrix for measurement errors (S_e) is given as a diagonal matrix with squared NER (Noise Equivalent Radiance) values at the diagonal entries. We assume the constant value 0.0005 [W/(m^{2}srμm)] for the whole spectral range considered in this study (Grassi et al., 2008). In the next steps we calculate radiances and brightness temperatures and then retrieve temperature profiles according to Eq. 3 and 7. As in case of the Chahine method, the quality of brightness temperature fits can be derived from the root mean square deviation between observed and modeled brightness temperatures according to Eq. 4.

The retrieval error of temperature profiles for Bayesian approach is estimated from calculations of temperature profiles from the spectral radiances with the NER (brightness temperatures – Fig.3). Radiances are calculated using the same temperature profile 'true' as in case of Chahine. Fig.4 shows the temperature profile uncertainty (the retrieval error) when using the Bayesian approach (solid line). The temperature retrieval error oscillates around 1 K for altitudes between 62 km (100 mb) to 74 km (5 mb) and from 81 km (1 mb) to near 92 km (0.07 mb). The 2 K temperature uncertainty peaks at higher altitudes near 78 km (2 mb) as it is for the Chahine method (4 K). Then the 4 K error is also observed above 95 km. Below 62 km the temperature uncertainty increases to 12 K with lowering altitude down to 56 km (300 mb). Below 56 km we do not consider the error because we do not have any information about the temperature structure due to very weak weighting function contributions (almost 0) (Fig.2b). Above 56 km the similar behavior of the temperature error has been found for the Chahine method. Comparing two curves we find that the Chahine method introduces smaller temperature uncertainties between 56 km and 62 km than the Bayesian approach. Thus, we

conclude that the Chahine method can describe the mesosphere at low altitudes (56 – 62 km) with better accuracy than the Bayesian approach.

6. Analysis of results

For the Chahine and Bayesian approaches we use the same initial temperature profiles presented in Fig.1 in the retrieval. In the Bayesian method the 'a priori' profile is different from the initial temperature profile. Fig. 5 illustrates a scatter plot of temperature values for altitudes between 56 - 98 km (300 and 0.03 mb) obtained by the two retrieval methods. Each color represents temperatures for the 5 altitude ranges: 56 – 60 km (purple), 60 – 70 km (blue), 70 – 80 km (green), 80 – 90 km (red), 90 – 100 km (black). The best agreement is observed for temperatures between 230 – 210 K which mainly correspond to altitudes between 70 – 77 km. From 210 – 180 K (80 – 100 km), the differences between temperatures increase to ~10 K. In the altitude range from 60 – 70 km Chahine temperatures are up to 10 K larger than Bayesian ones.

The largest inconsistency greater than 20 K is found for altitudes below 56 km. The retrieval errors for the Chahine and Bayesian methods are 6 K and 12 K respectively at this altitude (cf. Fig.4). The Chahine's method predicts much larger temperatures by about 30 K than for the Bayesian approach at these altitudes. The inconsistency (spread around solid line) at the bottom boundary (56 km) could be as result of sensitivity of cloud top altitude and of weighting functions. This altitude is very critical for both methods. Small contribution of weighting functions and top altitude of clouds could be main factors in the retrieval of consistent temperature profiles in the altitudinal range 50 – 60 km (purple) and 90 – 100 km (black).

We also plot the temperature differences from Bayesian and Chahine methods as a function of altitude (Fig.6). We constrain our plot to altitudes above 56 km and below 98 km. We present all 18 measurements thus there are 18 points at each altitude. The black dashed – dotted lines are the standard deviations of temperature differences. The standard deviations are ~2 K for altitudes from 70 to 77 km which is consistent with Fig.5. For higher altitudes than 77 km standard deviations increase to ~5 K.

Below 70 km standard deviations increase to ~7 K near 65 km. The differences between temperatures increase deeper in the atmosphere downward to 56 km (300 mb) with the standard deviation larger than 15 K. The large temperature differences between two

methods are due to the retrieval uncertainty. At 56 km the standard deviations are within the sum of the retrieval errors.

Fig.7 presents temperature differences between the Bayesian and Chahine method as a function of latitude. Mostly, the absolute temperature difference range that are retrieved from measurements listed in Tab.1 is in the order of 7 K (with sometimes $T_B<T_C$ or vice versa). For some measurements in the mid-latitude region the Chahine temperatures are higher than for Bayesian approach which is also evident in Fig.6 for altitude close to 58 km (200 mb). For the cold collar region, the variations between temperatures decrease to ~10 K. Poleward of 80°S, Bayesian temperatures are larger than Chahine ones and the difference between them increases with absolute latitude. We also observe a warmer atmosphere obtained using Bayesian approach for the low latitude region from 10°S - 25°S.

From our results presented in Fig.6 and Fig.7 we conclude that both methods are applicable to sound the atmosphere from 68 km to 98 km within 5 K of accuracy. However, after tests for convergence to initial profiles at boundaries we find that the Chahine method allows to obtain the reasonable temperature profiles up to ~90 km (~0.2 mb). We obtain good agreement within 9 K also for lower altitudes downward to 58 km. The Bayesian approach seems to be the better method to retrieve thermal profiles at altitudes higher than 62 km (100 mb) because the retrieval uncertainty range is less than 2 K (Fig.4). Chahine method, on the other hand, is more appropriate to be used in the lower mesosphere, especially between 56 and 62 km where the retrieval error does not exceed 6 K (Fig.4). The relaxation method is fast and robust, but the analysis of error is not well documented in previous works compared to the Bayesian approach. However, the Bayesian method is very time consuming because of required weighting function matrix calculations at each iteration.

Fig.8 illustrates observed and retrieved brightness temperature spectra for some VIRTIS radiance measurements. Four measurements performed at equatorial (2°S), mid (35°S), high (cold collar, 74°S), and polar (85°S) latitudes are selected from Tab.1. Retrieved spectra (and temperature profiles, cf. Fig. 9) consider the latitude-dependent cloud parameters given in Tab.2. The achieved overall quality of fits in terms of rmsd is indicated in each display. The smaller rmsd, the better the fit of the model. However, it is necessary to take into account the noise in the observations. The rmsd calculated for model radiances with NER and without in the considered spectral range is around 2.25 K. We obtain the rmsd approximately 2 K for all measurements using the Bayesian approach. The quality of fits of measured spectra by modeled spectra using Chahine method is slightly lower than in case of the Bayesian

approach, and at the selected equatorial latitude the rmsd (χ, cf. Eq. 4) exceeds 2 K. At the other selected latitudes, χ for both methods is always less than 2 K.

Fig. 9 shows retrieved temperature profiles for the four selected latitudes together with the corresponding initial profile taken from Fig.1. The same initial profile is used in both methods. Figures present modeled and observed brightness temperatures and derived temperature profiles, selected for equatorial, low-latitude, cold collar and polar regions. We observe good agreement between temperatures obtained by the Chahine method and Bayesian approach above ~56 km (~300 mb). Chahine temperatures are smaller than Bayesian below ~60 km and this disagreement increases downward to 56 km except at 35°S. Temperature profiles in the equatorial and low-latitude zones are very similar with except of altitudes above 80 km. At these altitudes the atmosphere in the equatorial belt is warmer than for the low-latitude region. The cold collar region with the temperature inversion between 60 - 70 km is well represented by results from both methods. Bayesian temperatures in the altitude range from 80 – 85 km show a small inversion which is more evident in the polar region using both methods.

7. Comparison with previous results

We find that the derived results from VIRTIS measurements are consistent with earlier results. Bayesian temperatures agree with the results from the VeRa instrument (Lee et al., 2012b, Tellmann et al., 2009) for the lower part of mesosphere below 65 km. Both Bayesian and Chahine temperatures show a second small inversion at higher altitudes around 85 km. The temperature inversion at around 85 km (0.5 mb) is also predicted by the GCM model for the Venus atmosphere (Fig. 5d in Migliorini et al. 2012). Similar inversion is also observed by the SPICAV although at 90 - 95 km (Bertaux et al., 2007, Piccialli et al., 2015). However, the temperature peak varies with altitude (Fig.1 in Bertaux et al. 2007).

We can distinguish three classes of temperature variations with altitude that depend on latitude. From 0° to around 55°S, Bayesian temperatures decrease with increasing altitude very quickly ~10K/km below 62 km (~100 mb). The similar lapse rate is observed by Chahine temperatures. The altitude of 62 km could be attributed to the boundary of tropopause. Above ~62 km up to 82 km (1 mb), retrieved temperatures decrease with increasing altitude more slowly (~2.5K/km) than below 62 km. The third range of temperature variations is from 82 km – 95 km. Apart from some small inversion features, temperatures are almost isothermal here. From 55°S to 75°S, temperature inversions at around 10 K appear at 62 km (~100 mb).

This is the so-called cold collar region. Thus, we suppose that the altitude of tropopause reduces to 58 km (~200 mb) in this latitude region and even lower to 56 km (~300 mb) for 80°S - 90°S which is in agreement with the results from the VeRa experiment (Tellmann et al., 2009). At 75°S - 80°S, the temperature inversions occur at 58 km (~200 mb). Then temperatures decrease with increasing altitude consistently with ~ 2 K/km up to ~82 km (1 mb). Our retrieval results also well coincide with Haus et al. (2014) who used VIRTIS-M measurements over the southern hemisphere but applied another retrieval algorithm (Smith relaxation method).

It is worth to note that our results also support earlier findings that the mesosphere above 70 km and poleward of 75°S is warmer by about 10 K compared to lower latitudes.

8. Summary and conclusions

We analyze atmospheric temperature profiles from 53 to 98 km (~700 mb - 0.03 mb) retrieved from nighttime measurements performed by the VIRTIS(M)-VEX instrument. However, above ~90 km (~0.2 mb) retrieved temperature profiles can be unreliable due to the large noise in the signal. The vertical thermal structure for selected observations is derived by using two retrieval methods including the Bayesian approach and the Chahine algorithm (relaxation method) adopted to the Venus atmosphere. A very good agreement between temperature profiles for both methods is obtained for atmospheric altitudes 59 – 98 km (150 mb and 0.03 mb) with the standard deviation less than 5 K. We can clearly observe the cold collar region with temperatures 230 K for atmospheric layers between 60 km and 65 km (~140 – 50 mb) and latitudes from 60°S to 75°S obtained from both applied retrieval methods. Over the polar region (85°S – 90°S) a hot structure with ~245 K is prominent between 60 – 65 km.

The two retrieval approaches with assumptions on clouds described in Tab.2 can investigate the thermal structure down to 56 km (300 mb) in the atmosphere but below 60 km (~140 mb) temperatures are with a large uncertainty.

As far as we know this is the first attempt to compare mesospheric temperature profiles that are retrieved by two independent methods. In most cases they give similar/comparable results, which provide more trust to the results and conclusions about physics derived from them. The main advantage of the optimal estimation method (Bayesian approach) is that it provides lower values of error estimates of the obtained results than Chahine method for atmospheric levels above 60 km. The disadvantage is much higher

processing time (or computing time) required by this method. The Chahine method allows us to study lower mesospheric thermal structure with a better accuracy compared to the Bayesian approach. However, the Chahine method weakly resolves the temperature inversions that may exist at high altitudes (~84 km) and that are observed in the results using the Bayesian approach.

Acknowledgments

PW would like to thank Alessandro Mura for their helpful hints in Matlab and prof. dr hab. Szymon Malinowski for his useful support. PW also thanks to prof. Rainer Haus for his comments.

References

Bertaux J.-L., A.-C. Vandaele, O. Korablev, E. Villard, A. Fedorova, D. Fussen, E. Quemerais, D. Belyaev, A. Mahieux, F. Montmessin, C. Muller, E. Neefs, D. Nevejans, V. Wilquet, J. P. Dubois, A. Hauchecorne, A. Stepanov, I. Vinogradov, A. Rodin & the SPICAV/SOIR team, (2007). A warm layer in Venus' cryosphere and high-altitude measurements of HF, HCl, H_2O and HDO. *Nature*, Vol. 450, 646 - 649, doi:10.1038/nature05974

Bougher S. W., D. M. Hunten, R. J. Phillips, 1997, Venus II--geology, Geophysics, Atmosphere, and Solar Wind Environment, Tom 1, The University of Arizona Press.

Carlson R. W., L. W. Kamp, K. H. Baines, J. B. Pollack, D. H. Grinspoon, Th. Encrenaz, P. Drossart and F. W. Taylor, (1993). Variations in Venus cloud particle properties: a new view of Venus's cloud morphology as observed by the Galileo Near-infrared Mapping Spectrometer. *Planet. Space Sci.*, vol. 41, No. 7, pp. 477 – 485.

Chahine, M. T., (1970), Inverse Problems in Radiative Transfer: Determination of Atmospheric Parameters, *J. Atmos. Sci.*, 27, 960-967.

García-Muñoz A., P. Wolkenberg, A. Sánchez-Lavega, R. Hueso, I. Garate-Lopez, (2013). A model of scattered thermal radiation for Venus from 3 to 5 μm. *Planetary and Space Science*, 81, 65–73, http://dx.doi.org/10.1016/j.pss.2013.03.007.

Grassi D., P. Drossart, G. Piccioni, N. I. Ignatiev, L. V. Zasova, A. Adriani, M. L. Moriconi, P. G. J. Irwin, A. Negrao, and A. Migliorini (2008). Retrieval of air temperature profiles in the Venusian mesosphere from VIRTIS-M data: Description and validation of algorithms, *Journal of Geophys. Res. – Planets*, vol. 113, E00B09, doi:10.1029/2008JE003075.

Grassi D., A. Migliorini, L. Montabone, S. Lebonnois, A. Cardesìn-Moinelo, G. Piccioni, P. Drossart, and L. V. Zasova, (2010). Thermal structure of Venusian nighttime mesosphere as observed by VIRTIS - Venus Express. *Journal of Geophys. Res. – Planets*, vol.115, E09007, doi:10.1029/2009JE003553.

Grassi D., R. Politi, N. I. Ignatiev, C. Plainaki, S. Lebonnois, P. Wolkenberg, L. Montabone, A. Migliorini, G. Piccioni, P. Drossart, (2014). The Venus nighttime atmosphere as observed by the VIRTIS-M instrument. Average fields from the complete infrared data set. *Journal of Geophys. Res. – Planets*, vol.119, 837 - 849, doi:10.1002/2013JE004586.

Haus, R., Kappel, D., Arnold, G., (2013). Self-consistent retrieval of temperature profiles and cloud structure in the northern hemisphere of Venus using VIRTIS/VEX and PMV/VENERA-15 radiation measurements. *Planet. Space Sci.* 89, 77 - 101, http://dx.doi.org/10.1016/j.pss.2013.09.020

Haus, R., Kappel, D., Arnold, G., (2014). Atmospheric thermal structure and cloud features in the southern hemisphere of Venus as retrieved from VIRTIS/VEX radiation measurements. *Icarus* 232C, 232-248, http://dx.doi.org/10.1016/j.icarus.2014.01.020

Ignatiev N. I., D. V. Titov, G. Piccioni, P. Drossart, W. J. Markiewicz, V. Cottini, Th Roatsch, M. Almeida, and N. Manoel, (2009). Altimetry of the Venus cloud tops from the Venus Express observations. *Journal of Geophys. Res. – Planets*, vol.114, E00B43, doi:10.1029/2008JE003320.

Kliore A.D., V.I. Moroz, G.M. Keating, (1985). The Venus International Reference Atmosphere, *Adv. in Space Res.*, 5, pp. 1–305 N11.

Lee Y.J., Venus cloud structure and radiative energy balance of the mesosphere, PhD thesis, 2012a.

Lee Y.J., Titov D.V., Tellmann S., Piccialli A., Ignatiev N., Pätzold M., Häusler B., Piccioni G., Drossart P., (2012b). Vertical structure of the Venus cloud top from the VeRa and VIRTIS observations onboard Venus Express. *Icarus*, vol. 217, 599–609, doi: 10.1016/j.icarus.2011.07.001.

Migliorini A., D. Grassi, L. Montabone, S. Lebonnois, P. Drossart, G. Piccioni, (2012). Investigation of air temperature on the nightside of Venus derived from VIRTIS-H on board Venus-Express. *Icarus*, vol. 217, 640-647, doi: 10.1016/j.icarus.2011.07.013.

Molaverdikhani, K., K. McGouldrick, L. W. Esposito, (2012). The abundance and vertical distribution of the unknown ultraviolet absorber in the Venusian atmosphere from analysis of Venus Monitoring Camera images. *Icarus* 217, 648 – 660, doi: 10.1016/j.icarus.2011.08.008.

Palmer, K. F., Williams, D., (1975). Optical constants of sulfuric acid – application to the clouds of Venus. *Applied Optics* 14, 208 – 219.

Piccialli A., F. Montmessin, D. Belyaev, A. Mahieux, A. Fedorova, E. Marcq, J.-L. Bertaux, S. Tellmann, A. C. Vandaele, O. Korablev, (2015). Thermal structure of Venus nightside upper atmosphere measured by stellar occultations with SPICAV/Venus Express. *Planet. Space Sci.*, http://dx.doi.org/10.1016/j.pss.2014.12.009

Piccioni G., P. Drossart, A. Sanchez-Lavega, R. Hueso, F. W. Taylor et al., (2007a). South-polar features on Venus similar to those near the north pole. *Nature*, vol. 450, 637 – 640, doi:10.1038/nature06209.

Piccioni G. et al. (2007b). VIRTIS: The Visible and Infrared Thermal Imaging Spectrometer, *Eur. Space Agency Spec. Publ.*

Rodgers, C. D., (2000). Inverse Methods for Atmospheric Sounding: Theory and Practice, *World Scientific*, Singapore.

Roos-Serote M., P. Drossart, T. Encrenaz, E. Lellouch, R. W. Carlson, K. H. Baines, F. W. Taylor, S. B. Calcutt, (1995). The thermal structure and dynamics of the atmosphere of Venus between 70 and 90 km from the Galileo – NIMS spectra. *Icarus* 114, 300 – 309.

Rothman, L. S., I. E. Gordon, A. Barbe, D. C. Benner, P. F. Bernath, et al., (2009). The HITRAN 2008 molecular spectroscopic database. *Journal of Quantitative Spectroscopy and Radiative Transfer*, 110, 533–572, doi:10.1016/j.jqsrt.2009.02.013.

Seiff, A., Schofield J. T., Kliore A. J., Taylor F. W., Limaye S. S., (1985). Models of the structure of the atmosphere of Venus from the surface to 100 kilometers altitude. *Advances in Space Research*, 5, 3–58.

Smith, W.L., (1970), Iterative Solution of the Radiative Transfer Equation for the Temperature and Absorbing Gas Profile of an Atmosphere, *Appl. Opt.*, 9, 1993-1999.

Stamnes K., S.-C. Tsay, K. Jayaweera, W. Wiscombe, (1988). Numerically stable algorithm for discrete-ordinate-method radiative transfer in multiple scattering and emitting layered media. *Applied Optics*, 27, 2502–2509.

Svedhem H., D. Titov, F. Taylor and O. Witasse, (2009). Venus Express mission. *Journal of Geophys. Res. – Planets*, vol. 114, E00B33, doi:10.1029/2008JE003290.

Taylor F.W., R. Beer, M. T. Chahine, D. J. Diner, L. S. Elson, R. D. Haskins, D. J. McCleese, J. V. Martonchik, and P. E. Reichley, (1980). Structure and Meteorology of the Middle Atmosphere of Venus: Infrared Remote Sensing From the Pioneer Orbiter. *Journal of Geophys. Res.*, vol. 85, NO. A13, 7963 - 8006.

Tellmann S., M. Pätzold, B. Häusler, M. K. Bird, G. L. Tyler, (2009). Structure of the Venus neutral atmosphere as observed by the Radio Science experiment VeRa on Venus Express. *Journal of Geophys. Res. – Planets*, vol.114, E00B36, doi:10.1029/2008JE003204.

Tellmann S., B. Häusler, D.P. Hinson, G.L. Tyler, T.P. Andert, M.K. Bird, T. Imamura, M. Pätzold, S. Remus, (2012). Small-scale temperature fluctuations seen by the VeRa Radio Science Experiment on Venus Express. *Icarus*, vol. 221, 471- 480, https://doi.org/10.1016/j.icarus.2012.08.023.

Winters, B., (1964). Line shape in the wing beyond the band head of the 4.3 μ band of CO_2. *Journal of Quantitative Spectroscopy and Radiative Transfer*, 4, 527–537.

Zasova L. V., I. A. Khatuntsev, V. I. Moroz and N. I. Ignatiev, (1999). Structure of the Venus middle atmosphere: Venera 15 Fourier Spectrometry data revisited. *Adv. Space Res.* Vol. 23, No. 9, pp. 1559-1568.

Zasova L. V., V. I. Moroz, V. Formisano, N. I. Ignatiev, and I. V. Khatuntsev, (2006). Exploration of Venus with the Venera-15 IR Fourier Spectrometer and the Venus Express Planetary Fourier Spectrometer. *Cosmic Research*, Vol. 44, No.4, pp. 349-363, https://doi.org/10.1134/S0010952506040083

Zasova L. V., N. Ignatiev, I. Khatuntsev, V. Linkin, (2007). Structure of the Venus atmosphere. *Planet. Space Sci.*, 55, pp. 1712 – 1728, doi:10.1016/j.pss.2007.01.011

Figure Captions

Fig.1. Initial temperature profiles taken from VIRA2. 'True' temperature profile is used for the error calculation in both methods.

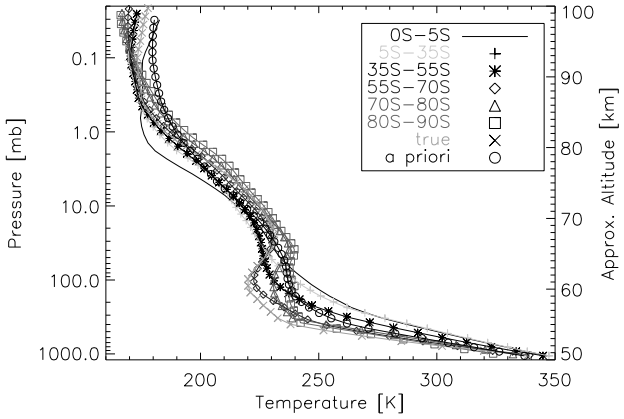

Fig.2. Weighting functions. a) calculated for the Chahine algorithm at selected wavelengths. b) calculated for Bayesian approach as the partial derivative of the forward model *F(x)* with respect to the state vector *x*.

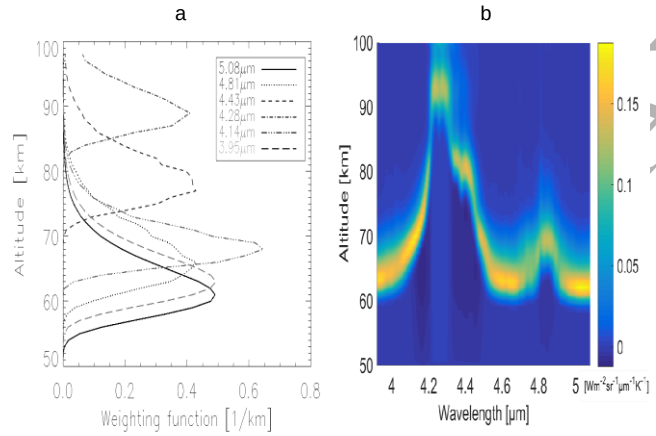

Fig.3. The 10 spectra with the generated Gaussian random noise used to estimate the retrieval uncertainty for both methods.

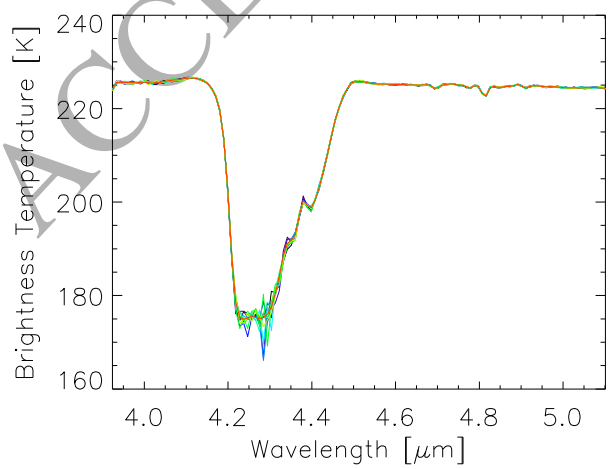

Fig.4. Retrieval error for temperature profiles obtained by the Chahine method (dashed line) and Bayesian approach (solid line).

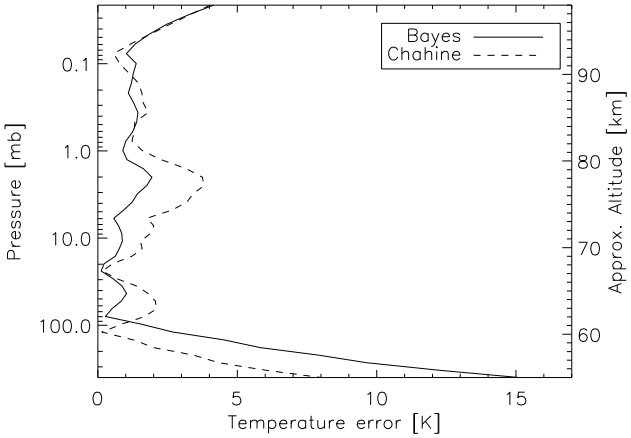

Fig.5. Scatter plot of temperature values at each atmospheric level obtained from the Bayesian approach and the Chahine method. Colors represent different altitudinal ranges: 56 – 60 km (purple), 60 – 70 km (blue), 70 - 80 km (green), 80 – 90 km (red), 90 – 100 km (black).

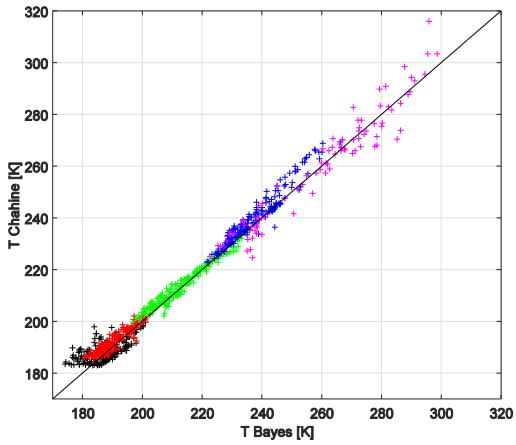

Fig.6. The difference between Bayesian and Chahine temperatures as a function of altitude. The black dashed-dotted lines present standard deviations of the difference between temperature profiles.

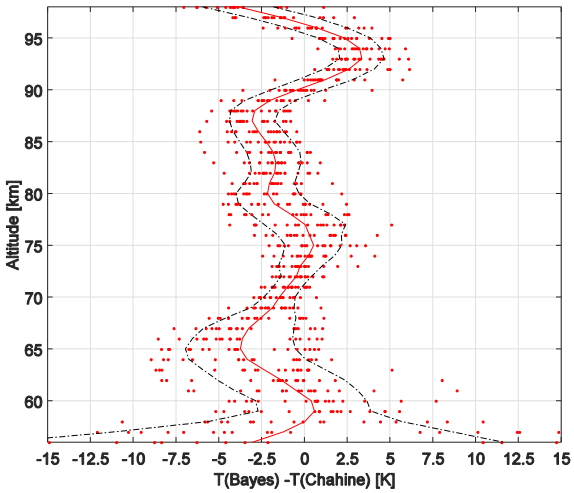

Fig.7. Scatter plot of temperature differences obtained from the Bayesian approach and the Chahine method as a function of latitude.

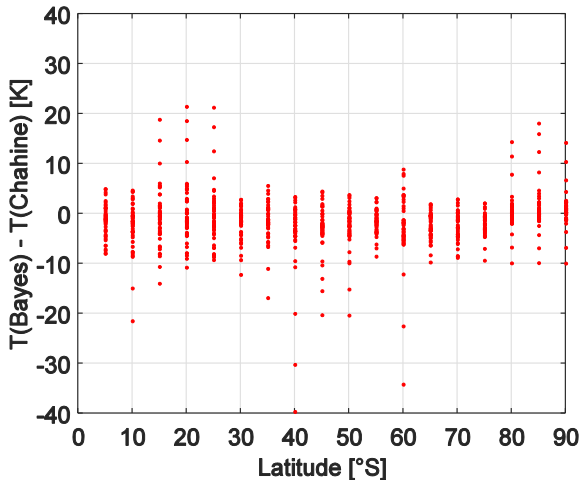

Fig.8. Comparison of measured and retrieved (model) brightness temperatures at different latitudes.

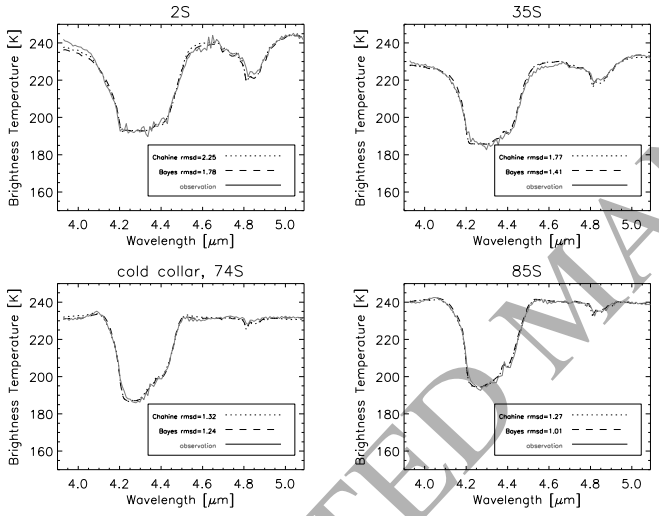

Fig.9. Comparison of initial and retrieved temperature profiles at different latitudes.

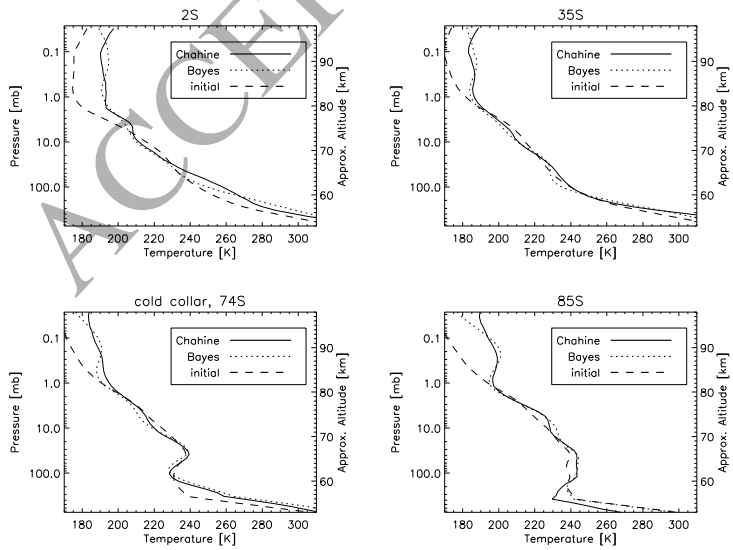

Table 1. Parameters of selected VIRTIS measurements.

Orbit (lines, frames)	Latitude	Orbit (lines, frames)	Latitude
23_02 (40, 464)	2°S	74_15 (8, 6)	49°S
23_02 (2, 514)	8°S	74_07 (3, 47)	53°S
23_02 (30, 590)	11°S	74_07 (3, 38)	58°S
23_02 (22, 651)	18°S	74_05 (10, 32)	63°S
23_02 (47, 751)	20°S	74_05 (6, 16)	66°S
78_17 (8, 27)	28°S	74_05 (11, 13)	74°S
76_15 (4, 37)	35°S	74_07 (29, 12)	80°S
76_11 (0, 37)	40°S	74_07 (33, 7)	83°S
74_15 (7, 58)	42°S	74_07 (44, 3)	85°S

Table 2. Latitude dependence of cloud properties.

Latitude [°S]	0-55	55 - 80	80 - 90
Scale height H [km]	3.8	2	1.5
Cloud top altitude z_{ct} [km]	70	65	61